www.czasopisma.pan.pl PAN POLSKA AKADEMIA NAUK www.journals.pan.pl

Arch. Metall. Mater. **64** (2019), 1, 401-412

DOI: 10.24425/amm.2019.126266

M. HOJNY*#, M. GŁOWACKI*,*****, P. BAŁA**,***, W. BEDNARCZYK**, W. ZALECKI****

A MULTISCALE MODEL OF HEATING-REMELTING-COOLING IN THE GLEEBLE 3800 THERMO-MECHANICAL SIMULATOR SYSTEM

The paper presents a multi-scale mathematical model dedicated to a comprehensive simulation of resistance heating combined with the melting and controlled cooling of steel samples. Experiments in order to verify the formulated numerical model were performed using a Gleeble 3800 thermo-mechanical simulator. The model for the macro scale was based upon the solution of Fourier-Kirchhoff equation as regards predicting the distribution of temperature fields within the volume of the sample. The macro scale solution is complemented by a functional model generating voluminal heat sources, resulting from the electric current flowing through the sample. The model for the micro-scale, concerning the grain growth simulation, is based upon the probabilistic Monte Carlo algorithm, and on the minimization of the system energy. The model takes into account the forming mushy zone, where grains degrade at the melting stage – it is a unique feature of the micro-solution. The solution domains are coupled by the interpolation of node temperatures of the finite element mesh (the macro model) onto the Monte Carlo cells (micro model).

The paper is complemented with examples of resistance heating results and macro- and micro-structural tests, along with test computations concerning the estimation of the range of zones with diverse dynamics of grain growth.

Keywords: DEFFEM package, finite element method, Monte Carlo method, physical simulation, computer simulation, mushy-zone, extra-high temperatures

1. Introduction

In the last decade, an intensive development of integrated metallurgical processes, in which the strand is cast and rolled in the semi-solid state to shape and dimensions near the net product, could be observed. Conventional cold rolling is a long process and it is not energy efficient. Therefore, in the aspect of technology, some operations of the process should be simplified or eliminated, to enable the energy consumption or manufacturing costs to be reduced. Also, an advantageous environmental impact by reducing emissions of noxious dusts and gases cannot be neglected. Modern processes of integrated casting and rolling may be performed in various ways, depending on the companies that apply them. They also differ in details and parameters of the industrial plant. Therefore, the above factors (economical, environmental) determine the need for controlled rolling of strands cast. Hence, the results of a physical simulation of the technological process analysed or of numerical simulations will be useful to control the process parameters. The continuous development of new integrated casting and rolling processes forces the engineers to look for new methods and tools to allow engineering work to be effectively aided. The emergence of new type of computer controlled machinery in the market, capable of changing the experiment conditions automatically during its execution according to the assumed programme, allows the selected technological process to be physically simulated.

The purpose of the physical simulation is to reconstruct in the laboratory conditions the changes in temperature, strain and stress to which the material is subjected during the actual industrial process.

In physical simulations, small samples made of the same material that is applied in the actual production process are used. The evaluation of thermo-mechanical properties of samples, which are subjected to various physical simulation variants, is the basis for developing guidelines to enable the optimal operation parameters of the process line equipment to be determined. Therefore, the laboratory test results may be applied directly and transferred into the industrial practice. Therefore, numerical modelling is a very effective aid for engineering

* AGH UNIVERSITY OF SCIENCE AND TECHNOLOGY, FACULTY OF METALS ENGINEERING AND INDUSTRIAL COMPUTER SCIENCE, DEPARTMENT OF APPLIED COMPUTER SCIENCE AND MODELLING, AL. MICKIEWICZA 30, 30-059 KRAKOW, POLAND
** AGH UNIVERSITY OF SCIENCE AND TECHNOLOGY, FACULTY OF METALS ENGINEERING AND INDUSTRIAL COMPUTER SCIENCE, DEPARTMENT OF PHYSICAL AND POWDER METALLURGY, AL. MICKIEWICZA 30, 30-059 KRAKOW, POLAND
*** AGH UNIVERSITY OF SCIENCE AND TECHNOLOGY, ACADEMIC CENTRE FOR MATERIALS AND NANOTECHNOLOGY, AL. MICKIEWICZA 30, 30-059 KRAKOW, POLAND
**** INSTITUTE FOR FERROUS METALLURGY, 12-14 K. MIARKI STR., 44-100 GLIWICE, POLAND
***** THE JAN KOCHANOWSKI UNIVERSITY, FACULTY OF MATHEMATICS AND NATURAL SCIENCE, 5 ŻEROMSKIEGO STR., 25-369 KIELCE, POLAND

Corresponding author: mhojny@metal.agh.edu.pl

these processes, allowing the engineering costs and time to be substantially reduced. Due to its specificity and complexity, the numerical simulation of high-temperature steel processing is one of the most difficult simulations in the metal processing area. A comprehensive numerical model should include effects related to the steel solidification or effects related to the flow of liquid steel within the solidified skeleton [1,2]. The existence of adequate constitutive equations, allowing the plastic behaviour of steel in high temperatures to be determined, has an impact on the result of numerical computing [1,3]. Thermal effects, such as heat generation and flow, heat exchange with the environment, or the formation and accumulation of internal stress during a change of the state of aggregation are another important aspects [2]. In addition, the complexity of the numerical modelling process stems from four primary aspects. The first one is a complex nature of the model, which requires the application of partial models – mechanical, thermal, fluid mechanics, or the microstructure development. The second one is lack of many data concerning fundamental material and thermo-physical properties. Another aspect is a very large difficulty in conducting an experiment at such high temperatures. And finally, it is not possible to effectively carry out direct industrial measurements to additionally verify the developed models and methods. On the other hand, the continuously growing demand for high quality products obtained by metal working, forces us to look for new manufacturing processes, providing top quality products while minimizing the negative environmental impact, manufacturing costs, including costs of engineering new processes [4,5]. In order to comprehensively describe the material behaviour during its deformation at temperatures near the solidus line, the constructed mathematical model must be three-dimensional. Spatial models need to be applied because two fundamental zones exist at high temperatures: the solid and the semi-solid zone, which often have complex geometrical shapes. We can well say that now the most important problem related to modelling plastic behaviour of semi-solid steel is lack of appropriate mechanical and thermo-physical properties within the temperature range where both the liquid and the solid state exist together. It should be emphasised that not much information concerning the material state, in particular for steel can be found in the available literature. Reviewing specialist articles published during almost twenty recent years, one can find many papers on experiments [6-8] and modelling heating/deforming non-ferrous metals [9-11]. Most of the mentioned papers focused on thixotropic processes. The first findings concerning heating/deforming steel at very high temperatures were presented in recent years [12-17]. The main factor influencing this fact is the high level of liquidus and solidus temperatures of steel as compared to non-ferrous metals. Therefore tests of heating and deforming non-ferrous metals were easier to perform in laboratory conditions. In recent years, the growing capabilities of thermomechanical Gleeble 3800 series simulators, and more and more common access to such units, enables high-temperature steel tests to be performed in order to determine mechanical properties, or the physical simulation itself of a selected manufacturing process [18]. Therefore to solve problems related to the high-temperature processing of steel, comprehensive tests should be applied, including both physical tests with appropriate equipment, and mathematical modelling. It must mentioned that testing physical properties of, and heating and deforming samples with the semi-solid core is only possible to a limited extent, with strictly defined testing methodology. As a rule it comes down to deforming samples in the laboratory conditions, e.g. using the mentioned thermo-mechanical Gleeble 3800 simulator. The multi-scale model of resistance heating presented in this paper is an innovative and original approach to simulation of the first stage preceding the deformation in the semi-solid state, that is heating a sample to a set nominal test temperature. Its numerical implementation was included in the original DEFFEM [1] software. Its main purpose is to effectively support physical simulations performed with Gleeble 3800 simulators by limiting, among others, the number of costly experimental tests [1]. Also, the fact that additional information can be obtained, e.g. about the local cooling rates achieved at any point of the sample tested volume, is quite significant. It will enable, for instance, the phase constitution of microstructure to be modelled on the basis of "high temperature CCT diagrams" determined by the **LUMet** (**L**aser-**U**ltrasonic Sensor for In-Situ **Met**allurgy Microstructure Studies) module of the Gleeble 3800 simulator.

2. Experimental research methodology

Physical simulations of resistance heating and melting combined with controlled cooling were carried out with a Gleeble 3800 thermo-mechanical simulator in the Institute for Ferrous Metallurgy in Gliwice. Steel S3555 with the chemical composition presented in Table 1 was examined.

TABLE 1

Chemical composition of the tested steel, %

C	Mn	Si	P	S	Cr	Ni
0.16	1.26	0.26	0.011	0.009	0.14	0.06

The solidus and liquidus temperatures were 1465°C and 1513°C, respectively. Hexahedral samples, with dimensions of 10×10×124 mm (identified as type C), were used in the tests. Additionally, the application of a quartz shield, which would be applied primarily to protect the simulator's interior against a leak of liquid metal during the execution of the high-temperature experiment, was given up. This approach allowed disturbances [1] influencing the mechanism of heat transfer between the sample and the simulator's interior to be limited. Fig. 1 shows a C-type sample diagram along with the locations of measurement thermocouples (TC2-TC4), and the locations of five heat transfer zones, identified as from Z1 to Z5, respectively. The zones identified as Z2 and Z4 define the contact area of the sample and the copper grips. From the perspective of the formulated numerical model,

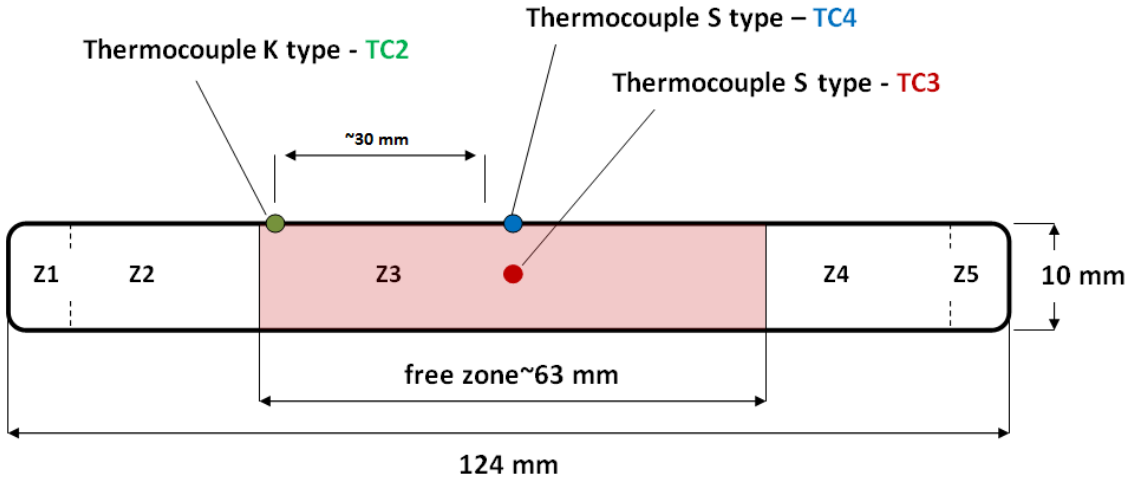

Fig. 1. Sample diagram along with the location of thermocouples (TC2-TC4) and heat transfer zones (Z1-Z5)

it is one of the key zones, where heat is intensively discharged to the tool. Zones Z1, Z3 and Z5 define the sample areas where free heat transfer to the environment occurs. The control thermocouple TC4, at the same time measuring the temperature at the sample surface is located at 1/2 of the sample heating zone length. Additional two thermocouples provide information on the temperature profile in the sample core (thermocouple TC3) and near the sample-copper grips contact (thermocouple TC2). The numerical sensors identified as NTC2, NTC3 and NTC4, respectively, in the numerical model correspond to the locations of actual thermocouples TC2, TC3 and TC4.

On the basis of the determined solidus and liquidus temperatures of the steel investigated, and also bearing in mind that as a result of resistance heating within the Gleeble 3800 simulator system the highest temperatures occur within the sample core, the following experiment programme was proposed. The first stage was heating the sample to the temperature of 1400°C at a constant rate of 5°C/s, followed by heating to the temperature of 1440°C at a rate of 1°C/s. The next stage was controlled cooling at a rate of 10°C/s to a nominal temperature of 800°C. At the last experiment stage the samples were cooled to the ambient temperature in the Gleeble 3800 simulator tool system. During the experiment, the temperature was recorded as indicated by the thermocouples (TC2 and TC4). The core temperature measurement (thermocouple TC3) was recorded up to the test nominal temperature of 1200°C. Within the temperature range 1200°C-1440°C, the core temperature was estimated on the basis of experimental data approximation. In addition, during the experiment, the electrical current intensity was recorded. The recorded characteristics of current intensity (Fig. 2) were the input data necessary for the execution of the computer simulation in accordance with the formulated numerical model presented in the following section.

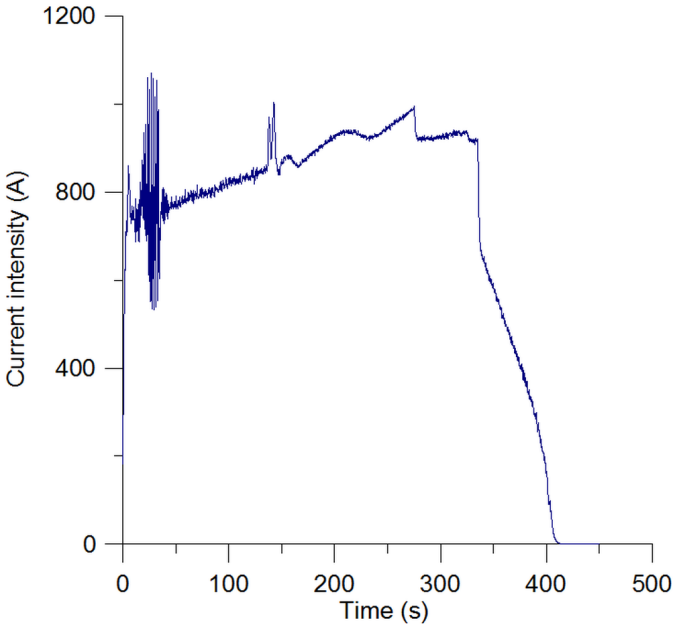

Fig. 2. Change of the current intensity versus time recorded during the experiment

3. Multi-scale model

3.1. Thermal model (macro solution)

The numerical model for the macro-scale is based upon the solution of the Fourier-Kirchhoff differential equation, with the existing internal voluminal heat source [1]:

$$\nabla^T \left(\lambda \nabla T\right) + Q = c_p \rho \frac{\partial T}{\partial \tau} \tag{1}$$

where:

- Q – rate of heat generation resulting from the current flow,
- ρ – steel density at a temperature T,
- c_p – specific heat,
- λ – vector of thermal conductivity distribution function,
- τ – time.

The accuracy of estimation of the temperature field distribution at any point of the tested sample volume depends primarily on the correct determination of the boundary conditions neces-

sary to solve the transient heat flow problem. The initial condition of 20°C was assumed in the form of the known temperature distribution t_0. In the presented numerical model, the boundary conditions were defined in each zone marked in Fig. 1 as Z1 to Z5, respectively, in the form of heat fluxes q_n:

$$q_n = \alpha_e(t - t_o) \tag{2}$$

where:

t_o – the temperature of the medium in contact with the area of the specific zone,

α_e – substitute heat-transfer coefficient for the specific zone.

In many studies related to the subject of heat transfer, contact effects are modelled with the heat transfer coefficient α. The proper selection of this coefficient is a significant problem, and the values given in numerous papers often differ by the order of magnitude. In practice, most often the coefficient values α have been determined by matching the temperature calculation results to the results of measurements carried out during the experiment. In the presented numerical model a constant substitute coefficient α of 5000 W/m^{2}K was assumed in the area of contact of the sample and the copper grips (zones Z1, Z2, Z4, Z5), and for the free zone (Z3) a value of 120 W/m^{2}K. The method of taking into account the emitted heat resulting from the electric current flow is the key component of the resistance heating model. The flow of electric current through a conductor is always accompanied by heat emission. It means that in components with a certain resistance, the electrical energy turns into the thermal energy. In the proposed solution the heat accompanying the electric current flow was included in the equation (1) as the power of internal heat sources Q. When modelling the heat generation resulting from the electric current flow, it was assumed that its equivalent in the numerical model would be a voluminal heat source with its power proportional to the square of electric current intensity I, resistance R, and the intensity function A selected experimentally [1]:

$$Q = A(\tau)[I^2(\tau)R(T)] \tag{3}$$

Analysing the process from the physical side, both the resistance R, and the current intensity I, depend on a number of parameters, in particular on the temperature T and time τ. During the resistance heating process, also the internal structure changes, which ultimately also changes the heat conduction conditions and the current intensity. The heat source efficiency is therefore a function of resistance R, which in turn depends on temperature T. It corresponds to a change in resistance R in the numerical model, and thereby a change in the efficiency of the internal heat Q sources. The numerical solution is complemented by the description of the solidification in terms of enthalpy with the approximation of the substitute thermal capacity [19,20], allowing for the heat generated as a result of the change in the state of aggregation in the model. The thermo-physical characteristics for the needs of the numerical simulation (macro model) were

TABLE 2

Thermo-physical properties of the steel tested

Temp. (°C)	Density (g/cm^3)	Thermal conductivity (W/(m K))	Electrical resistivity (10e-6 Ohm m)	Enthalpy (J/g)	Specific heat (J/(g K))	Latent heat (J/g)
1520	6.97717	33.44813	1.31344	1275.71312	0.81806	
1513.7	6.98222	33.33249	1.31337	1270.56868		50.97787
1500	7.13721	36.00007	1.20672	1131.80022	6.05028	96.93005
1486.24	7.20396	37.09981	1.16187	1072.07531		128.23126
1483.93	7.25349	35.0414	1.2285	1015.08179		150.54388
1480	7.2678	35.1107	1.22334	1001.52911	2.97105	167.01298
1465.4	7.29098	35.10308	1.21341	975.70594		211.36935
1465.22	7.29142	35.10561	1.2132	975.06483		241.82898
1460	7.29426	35.03964	1.21183	971.38423	0.70351	
1400	7.32673	34.28274	11.19571	929.49892	0.69173	
1280	7.39127	32.772	1.16112	847.72861	0.67016	
1240	7.41278	32.26891	1.14885	821.03032	0.66333	
1120	7.47759	31.76595	1.13619	794.59762	0.65679	
900	7.59809	27.99507	1.02669	604.41988	0.60943	
880	7.60917	27.7437	1.01833	592.23888	0.60632	
820	7.63921	27.19745	0.98473	554.9352	0.99814	
720	7.62059	31.21428	0.77952	452.16563	1.0585	
700	7.61719	32.55451	0.73238	421.67167	2.16441	
600	7.64982	34.2856	0.62394	327.04394	0.80251	
520	7.67936	35.47328	0.5478	266.15472	0.72132	
420	7.71658	37.80282	0.44923	195.61239	0.64602	
300	7.75724	40.87627	0.34353	122.39202	0.57492	
200	7.7895	44.03823	0.26323	67.46756	0.52339	
120	7.81421	46.97471	0.20505	27.08885	0.48655	
80	7.82621	48.58644	0.17808	7.95299	0.46994	
25	7.84248	50.93719	0.14341	7.95157	0.44669	

determined on the basis of the chemical composition of the steel tested, using commercial software JMatPro v.8. Table 2 presents calculated thermo-physical relationships, which, after approximation with polynomial functions were implemented as separate subroutines in the numerical model. The evolution of thermo-physical properties was executed for each Gauss point of the integrating procedure.

3.2. Grain growth model (micro)

The micro model of grain growth is based upon the Monte Carlo method [1,21]. Although the Monte Carlo method is universally known, no comprehensive approach to the grain growth simulation in complex processes of heating-melting-cooling has been developed until now. The MC algorithm is probabilistic, and is based upon minimization of system energy. A local change of energy E is calculated with the Hamiltonian:

$$E = J\sum_{\langle i,j\rangle}\left(1-\delta_{ij}\right) \tag{4}$$

where:

- J – is the grain boundary energy,
- i – is the cell ranging from 1 to the total number of cells,
- j – is the neighbour of site i ranging from 1 to the number of neighbors of i,
- δ – is the Kronecker delta.

A characteristic feature of the micro model is taking into account in the simulation of the remelting process (formation of the mixed liquid-solid phase) and the influence of the high temperature gradient, which forms within the sample volume, on the grain growth dynamics. This effect has been achieved by applying a special boundary mobility function, which takes into account the change in probability depending on temperature $B_m(T)$. This approach allowed the sample volume to be included comprehensively in numerical simulations, and the grain size to be estimated in each of the sample zones characterized by a different temperature profile in a complex heating-melting-cooling cycle. The central area of the sample shows the biggest dynamics of temperature changes. In this area the maximum temperature values (function $B_m(T) = 1$) are achieved, and decline towards the areas where the temperature, as a result of intensive cooling, reaches much lower values (function $B_m(T) = 0$).

The kinetics of grain growth is simulated by random selections of cells and attempts to change their states by changes of the identifier Q describing the affinity to a specific grain orientation, to the identifier of the neighboring grain. Cells located within the grain that do not have a neighborhood belonging to a different grain type, cannot change their state. When the chosen cell is subjected to an attempt at state change, a random choice is made of one state from all the neighbouring states. Taking into account the boundary mobility function, the change of state is accepted with a probability of P:

$$P = \begin{cases} B_m\left(T\right)e^{-\frac{\Delta E}{kT}} \Delta E > 0 \\ B_m\left(T\right)\Delta E \le 0 \end{cases} \tag{5}$$

where:

- kT – is the modelling parameter,
- ΔE – is the change of energy due to the change of orientation.

The simulation of heating-melting-solidification is executed within the model as follows. When the temperature of the sampled cell i, is equal to or higher than the assumed melting temperature $T \geq T_{melting}$, melting is simulated by random assignment of a state to cell i that is different from the states of its neighbours. A degradation of the grain structure and increase in accumulated energy occurs. For the solidification process, a normal grain growth algorithm is used, through a random selection of the state (of the grain identifier) from among the states of neighbouring cells, the reduction of energy and the formation of a new grain from at least two neighbouring cells. Coupling the macro-model with the micro-model is established by the interpolation of node temperatures of the finite element mesh on the Monte Carlo cells for the selected integration steps. At the present stage of the model development, feedback from the micro to the macro model was not considered. The linear relationship between the MC algorithm step quantity and the actual simulation time was assumed in the computation.

4. Examples of results

4.1. Modelling the resistance heating

Numerical simulations of resistance heating combined with melting and controlled cooling were performed in line with the experiment schedule presented in Section 2. The objective of the simulation was to analyse the possibilities for a response of the numerical model in terms of the correct prediction of the distribution of temperature fields within the volume of the sample tested. Figs 3-8 show the computed temperature fields for six selected simulation stages, i.e. after 50, 100, 200, 280, 300 and 330 seconds of the heating process at a rate of 5°C/s and 1°C/s, respectively. On the other hand Figs 9 and 10 show the temperature fields for 370 and 400 seconds of controlled cooling at a rate of 10°C/s.

Analysing the obtained results one may observe a forming intensive temperature gradient along the heating zone of the whole sample. The areas located within the immediate impact of the copper grips (zones Z1, Z2, Z4 and Z5, Fig. 1) achieve their maximum temperature at the surface not exceeding 33°C (Fig. 8).The free area of the sample (zone Z3), which is characterised by the highest intensity of the heat emitted, achieves the temperatures at the sample surface of about 420°C right next to the tool, achieving the maximum of 1441°C in the half of the sample heating zone length (Fig. 8).

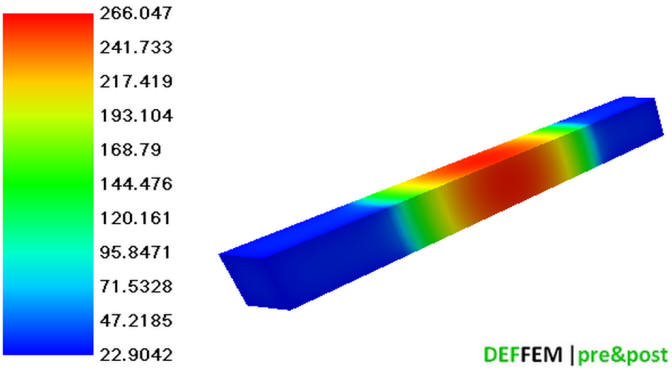

Fig. 3. The temperature field during the process of heating at a rate of 5°C/s (50-th second of the process, NTC4 = 260°C)

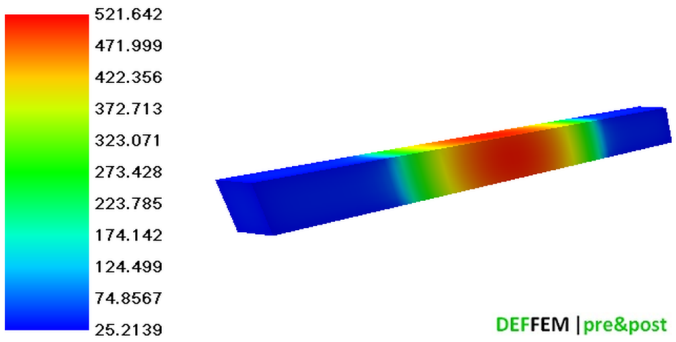

Fig. 4. The temperature field during the process of heating at a rate of 5°C/s (100-th second of the process, NTC4 = 510°C)

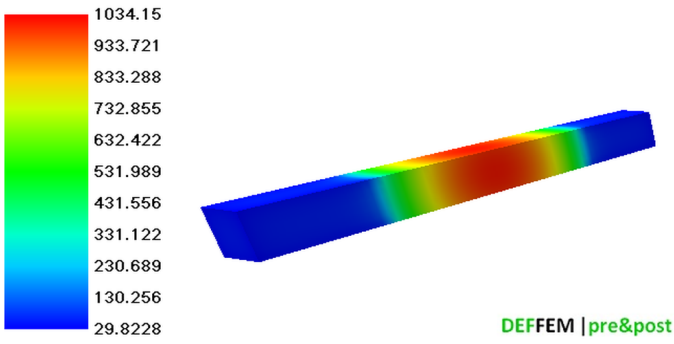

Fig. 5. The temperature field during the process of heating at a rate of 5°C/s (200-th second of the process, NTC4 = 1011°C)

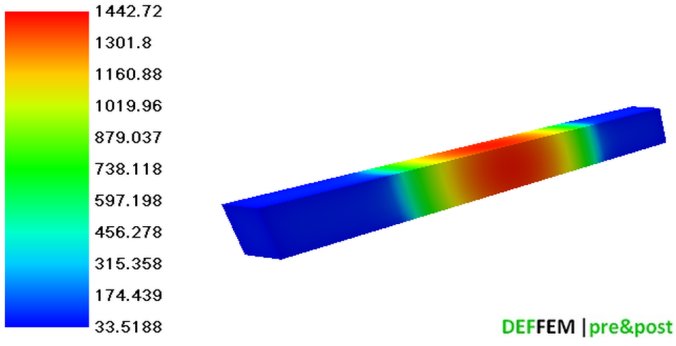

Fig. 6. The temperature field during the process of heating at a rate of 5°C/s (280-th second of the process, NTC4 = 1410°C)

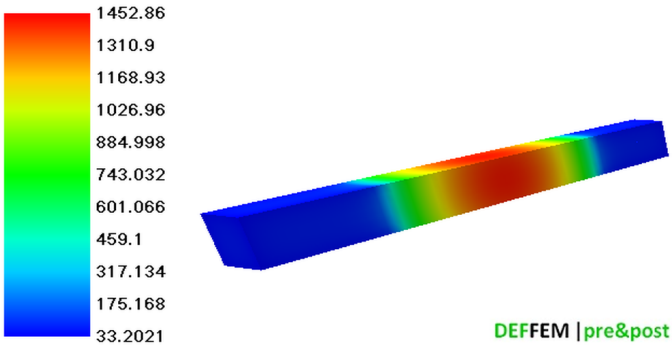

Fig. 7. The temperature field during the process of heating at a rate of 1°C/s (300-th second of the process, NTC4 = 1420°C)

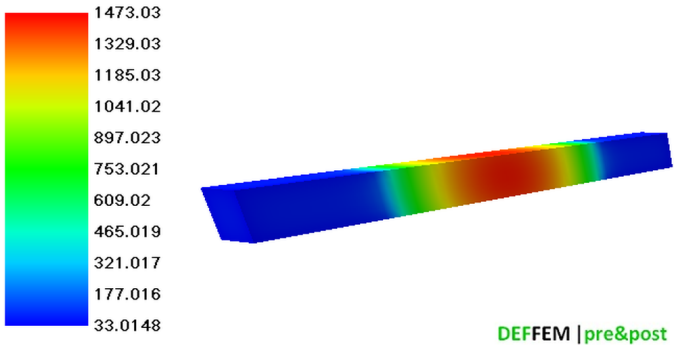

Fig. 8. The temperature field during the process of heating at a rate of 1°C/s (330-th second of the process, NTC4 = 1441°C)

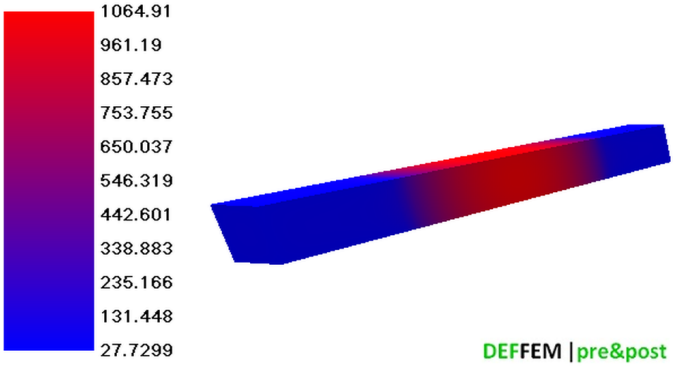

Fig. 9. The temperature field during the process of cooling at a rate of 10°C/s (370-th second of the process, NTC4 = 1041°C)

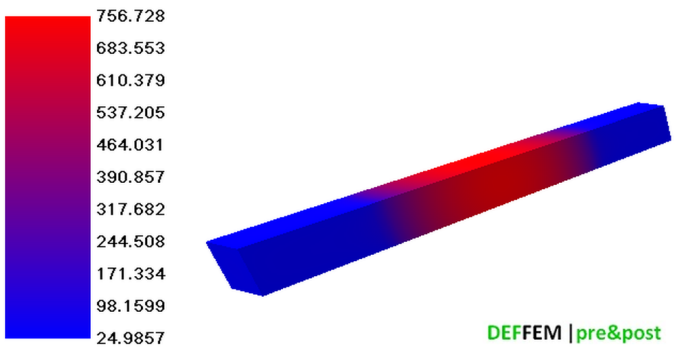

Fig. 10. The temperature field during the process of cooling at a rate of 10°C/s (400-th second of the process, NTC4 =740°C)

The changes of temperatures versus time obtained experimentally and by numerical computing (Fig. 11) show a good conformity (the readings of thermocouple TC4 and numerical sensor NTC4). Slight differences appear for the readings of thermocouple TC2 and its corresponding numerical sensor NTC2 near the sample-copper grip contact.

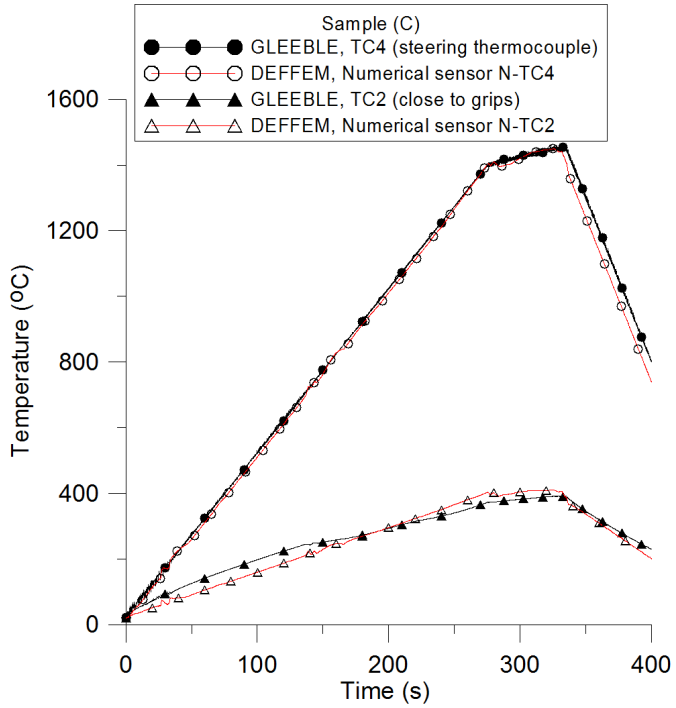

Fig. 11. Changes in temperature versus time obtained by physical and numerical simulations according to the readings of thermocouples (TC4, TC2) and numerical sensors (NTC4, NTC2)

Analysing the obtained temperature fields presented in Fig. 3 to Fig. 10, it was found that as the nominal test temperature increased, the temperature difference between the sample surface and its core increased. After 50 seconds of heating, the difference between the sample surface and its core was about 6°C (Fig. 3), reaching its maximum value of about 33°C at the final stage of slow heating (Fig. 8), and just before the controlled heating stage. This difference decreased to about 23°C (Fig. 9) after cooling to a temperature of 1041°C, and next to about 16°C at the last stage of controlled cooling (Fig. 10). As shown by additional experiments, implementing modified heating schedules does not eliminate the occurring temperature gradient in the cross-section. Table 3 shows examples of temperature measurement results at the sample surface (thermocouple TC4) and the corresponding values of core temperature (thermocouple TC3). The experiments were performed for three various heating rates to a temperature of 1400°C. Further heating in each of the experiments was performed at a rate of 1°C/s to a temperature of 1440°C. Analysing the obtained temperature differences between the readings of thermocouples TC3 and TC4 (Table 3), one can find that the obtained values do not differ fundamentally and they show a suitable conformity. For the temperature of 1200°C in all heating variants a stabilized temperature difference between the sample core and its surface of about 26°C was obtained, achieving its maximum value of 42°C (approximated value) for the temperature of 1440°C.

TABLE 3

Comparison of the selected temperatures measured as indicated by thermocouples TC3 and TC4 (experiment)

Heating rate 5°C/s (first stage)						
Temperature [°C]	100	300	500	800	1200	1440
TC3, [°C]	106.22	308.96	509.32	816.14	1226.81	1481.89
TC3-TC4, [°C]	***6.22***	***8.96***	***9.32***	***16.14***	***26.81***	***41.89***
Heating rate 10°C/s (first stage)						
TC4, [°C]	100	300	500	800	1200	1440
TC3, [°C]	104.15	308.15	508.75	815.07	1226.56	1482.45
TC3-TC4, [°C]	***4.14***	***8.15***	***8.75***	***15.07***	***26.56***	***42.45***
Heating rate 20°C/s (first stage)						
TC4, [°C]	100	300	500	800	1200	1440
TC3, [°C]	105.68	305.40	507.37	816.32	1226.22	1482.13
TC3-TC4, [°C]	***5.68***	***5.40***	***7.37***	***16.32***	***26.22***	***42.13***

With regard to the obtained numerical computing results for the heating rate of 5°C/s presented in Table 4, the obtained temperature differences between the readings of numerical sensors NTC3 and NTC4 show a good conformity with the values measured in the experiment (Table 3). The temperature difference between the sample core and its surface of about 27°C was obtained for the temperature of 1200°C. The temperature difference reached its maximum value of about 33°C for the temperature of 1440°C. This value was lower by 9°C than the value approximated on the basis of the experiment. The total relative error for the presented five temperatures (temperature of 1440°C was not included) between the measured and computed values was 0.015%.

TABLE 4

Comparison of the selected temperatures computed according to the readings of numerical sensors NTC3 and NTC4

Heating rate 5°C/s						
NTC4, [°C]	100	300	500	800	1200	1440
NTC3, [°C]	102.08	306.96	511.42	818.41	1227.52	1473.03
NTC3-NTC4, [°C]	***2.08***	***6.96***	***11.42***	***18.41***	***27.52***	***33.03***

4.2. Grain growth modelling

Numerical simulations of grain growth were focused on the selection of an appropriate boundary mobility function, for the correct estimation of the range of zones with a diversified dynamics of grain growth within the volume of the sample tested.

In the numerical computing the boundary mobility function of the second and third degree was applied:

$$B_m(T) = \frac{(T-20)^n}{(T_l-20)^n} \tag{6}$$

where:

T – temperature of subsequent cells,
T_l – liquidus temperature of the steel tested,
n – function degree.

Other parameters for the purposes of the simulation were assumed as follows:

– parameter kT in equation (5) equal to 0.4,
– number of Q states of 54.

Due to very long computing times if the whole sample was considered the solution domain, the grain growth was modelled within a selected sample volume. On the basis of microstructure examinations and the existing symmetry plane Z, the proposed size of the solution domain was 40 mm. Fig. 12 shows a sample view with the generated initial structure on the longitudinal section of the sample (for Q = 54) with the marked area included in the computing.

The macro- and micro tests were conducted in the selected longitudinal sections in the sample axis, starting from the centre of the heating zone identified as 0 mm, at a distance of 5, 10, 15, 20, 25 and 30 mm, respectively.

The results of temperature field distributions presented in the previous section show that zones, where diverse cooling

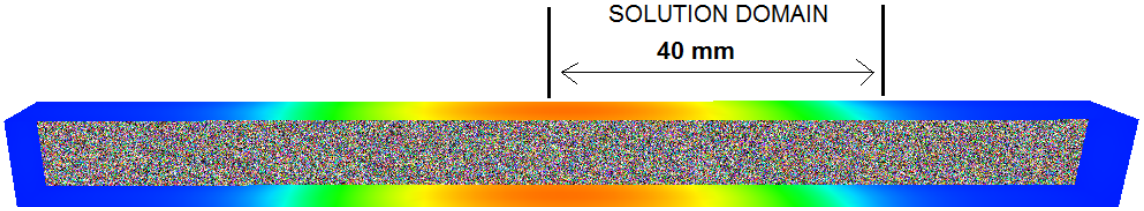

Fig. 12. The initial structure of the selected longitudinal section along with the marked solution domain

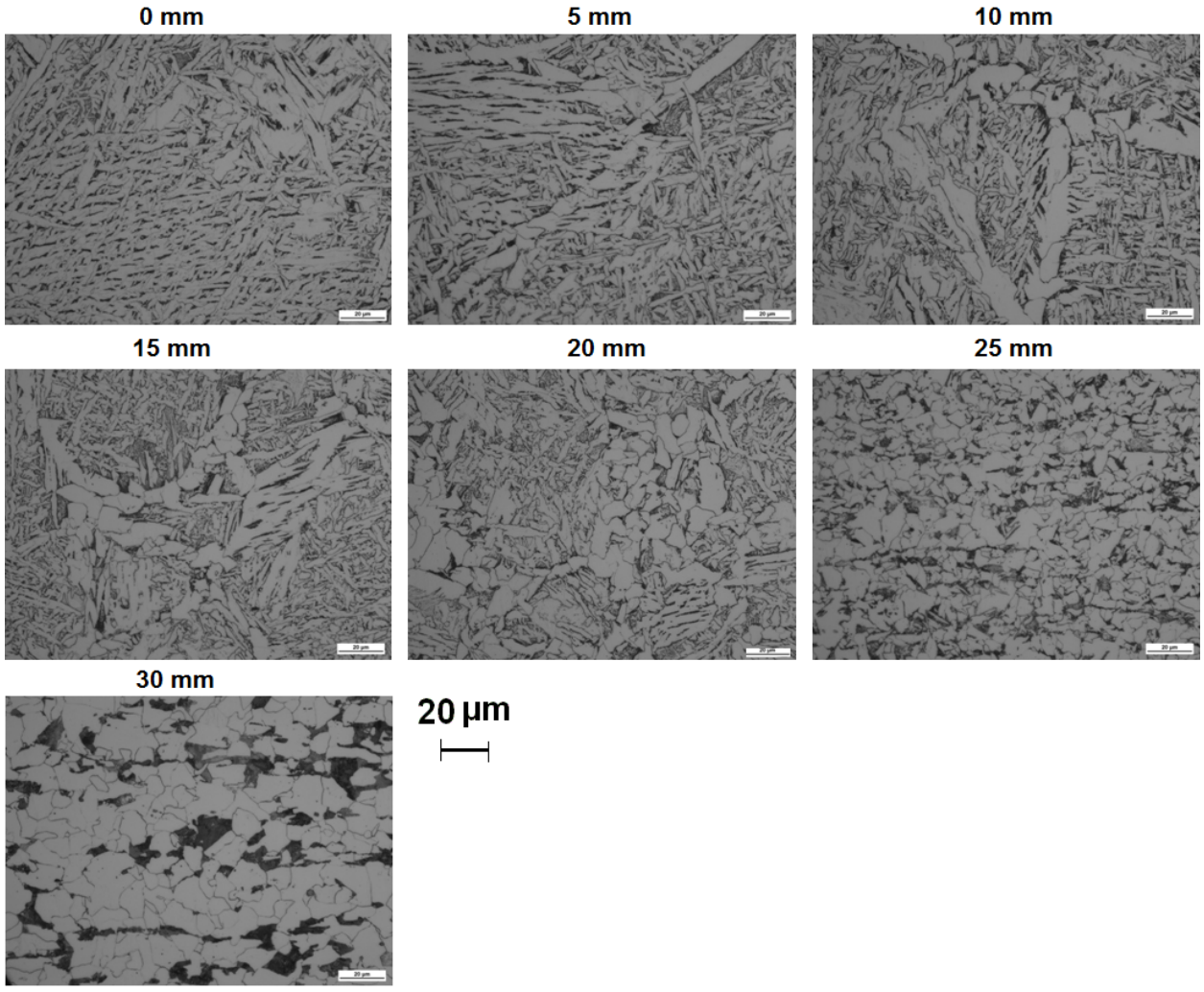

Fig. 13. Microstructure of the tested sample in the selected longitudinal sections

rates are achieved, exist within the sample volume [1]. This in turn translates into a diversified structure in terms of phases within the sample volume (Fig. 13), as well as the occurrence of zones with a diversified dynamics of grain growth (Fig. 14). The microstructure consists mainly of ferrite (white needles) and perlite. Precipitates of polygonal ferrite are visible along border of prior austenite grain (from sample center to distance of 20 mm). The dark areas close to ferrite are trials of perlite. The fraction of needles-shaped phase is caused by rapid cooling of the sample from very high temperature (~1440°C). It reminds Widmastatten ferrite. The microstructure in the distance 25 and 30 mm from sample center consists of bands of ferrite and perlite.

The analysis of the obtained macrostructures reveals that zones with a diversified dynamics of grain growth exist within the sample volume (Fig. 14). The area of the sample centre and within a distance of 5 mm (the highest temperature range) is characterised by a structure, in which the largest grains exist (coarse structure). Moving towards the copper grips (decreasing temperature), at a distance of 10, 15 and 20 mm from the sample centre, the structure becomes finer, with a fading visible grain boundary. At a distance of 25 mm from the sample centre, the obtained structure is virtually the original structure.

Fig. 15 shows the macrostructure of the sample tested in the longitudinal section, at the same time it corresponds to the assumed area included in the numerical computing (40 mm). On the basis of the conducted analyses of the macrostructure (Fig. 14 and Fig. 15) and numerical computing, it was proposed to divide the sample into four basic zones:

– the melting zone (**MZ**), where local melting of the sample occurs, and depending on the obtained local cooling rates it is followed by a new grain growth or an epitaxial growth at the grain boundary within the melting zone (the beginning of the transition zone **TZ**),

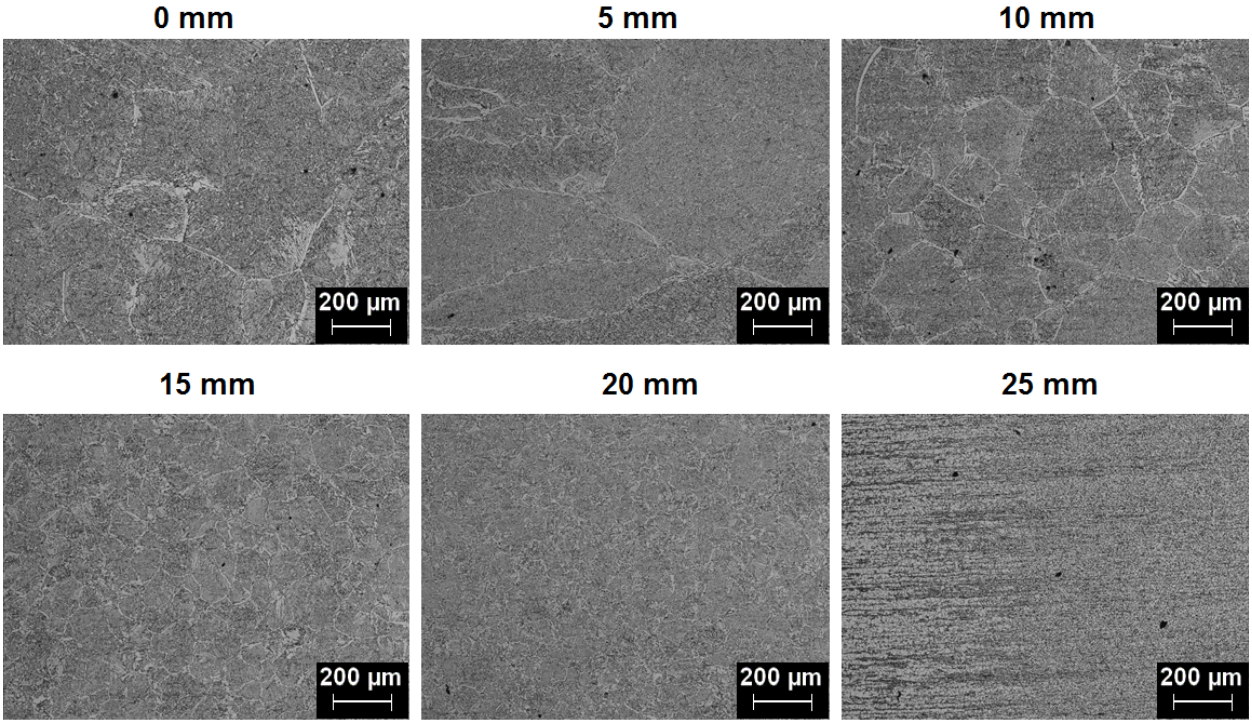

Fig. 14. Macrostructure of the tested sample in the selected longitudinal sections

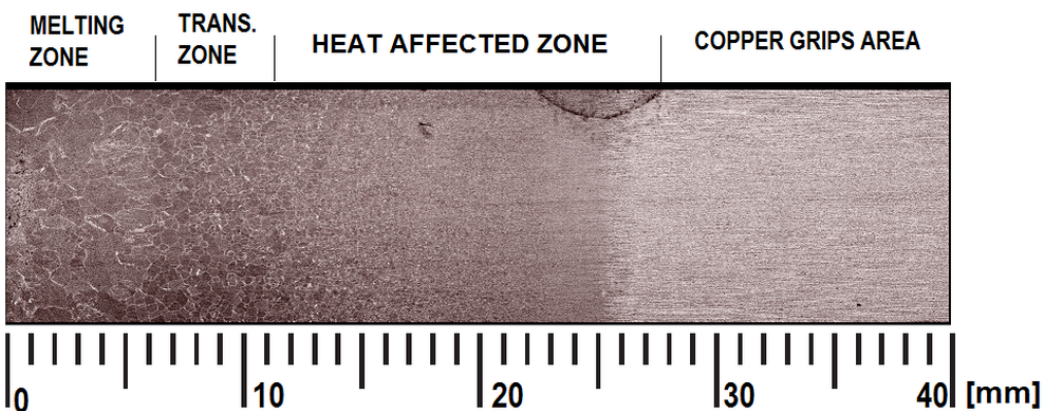

Fig. 15. Macrostructure of the tested sample in a longitudinal section with marked zones with a diversified dynamics of grain growth

– the transition zone (**TZ**), where no local melting occurs, but which features a dynamic grain growth as a result of high temperatures achieved within this area,
– the heat affected zone (**HAZ**), characterized by a low dynamics of grain growth, due to a much shorter range of the achieved temperatures,
– the copper grip impact area (**CGA**), which due to the low achieved temperature range features a negligible dynamics of grain growth.

Fig. 16 and 17 show the computed macrostructures in a longitudinal section in the solution domain sample axis, for the selected four process stages and the mobility function of the second and third degree, respectively. Analysing the virtual macrostructures obtained at the final heating stage, one can unambiguously state that thanks to applying the third degree mobility function a much larger area is obtained, and that the grain growth dynamics in this area is negligible, which results in retaining the original structure condition. Going to the sample melting stage, for the subsequent two macrostructures one can observe the formation of an area where a mixed phase, comprising solid and liquid phases, exists. The last macrostructure presents the condition after completion of the controlled cooling process, where due to the obtained high cooling rates a slightly fine structure was obtained compared to the structure obtained at the end of the heating stage.

Fig. 18 shows the estimated ranges of macrostructure zones with a diverse dynamics of grain growth obtained by experiment and numerical computing performed for two mobility functions. The average value of grain number per 1 mm^2 and the average value of grain cross-section area were adopted as a criterion defining the scope of occurrence of individual zones. The maximum relative error not exceeding 20-25% was assumed in the analyses. The ImageJ software was applied to analyse the images. This is an open source image processing program designed for scientific multidimensional images. It arises from the conducted investigations that the application of the third degree mobility function is the best reproduction of the experiment. Therefore we can conclude that the development and implementation of more complex mobility functions will allow the macrostructure zones with a diverse dynamics of grain growth to be more precisely estimated.

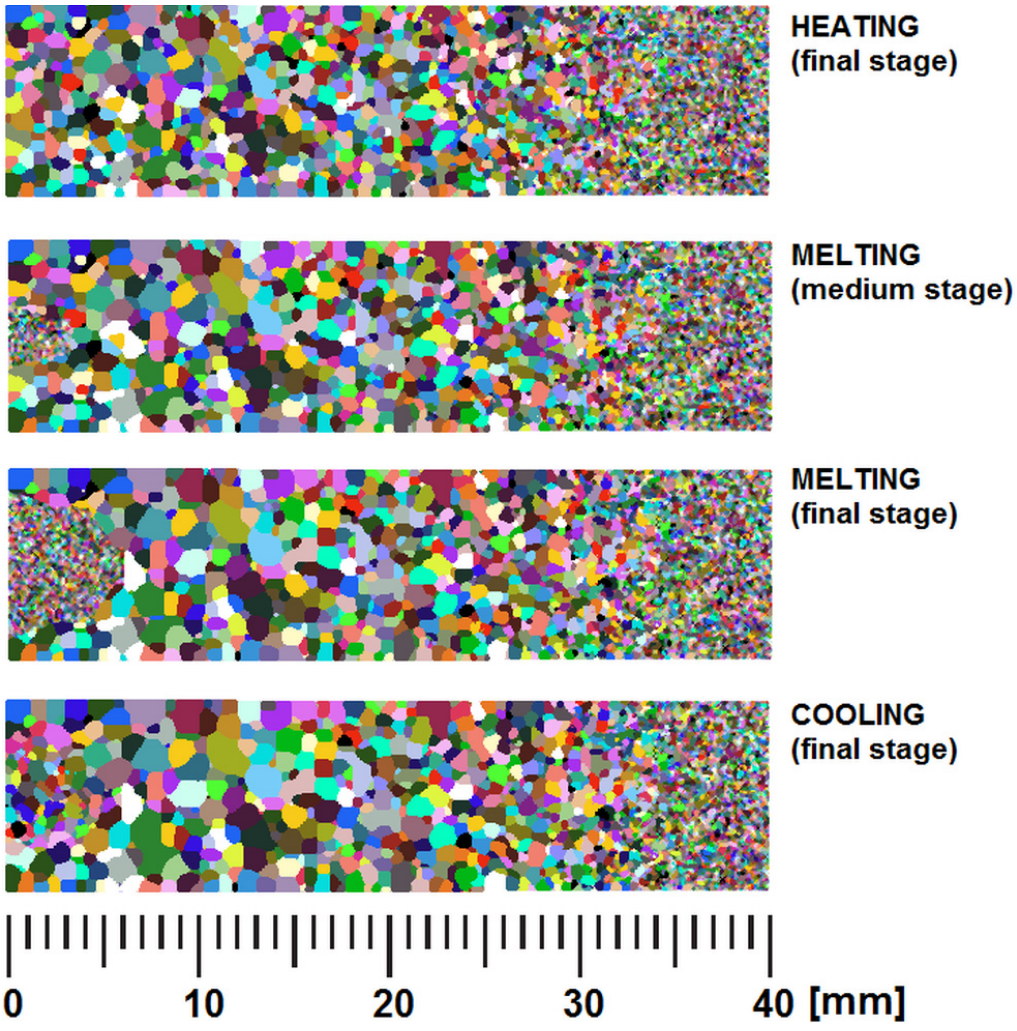

Fig. 16. Virtual macrostructure of the sample in the longitudinal section in the sample axis for the selected four process stages (*second degree* boundary mobility function)

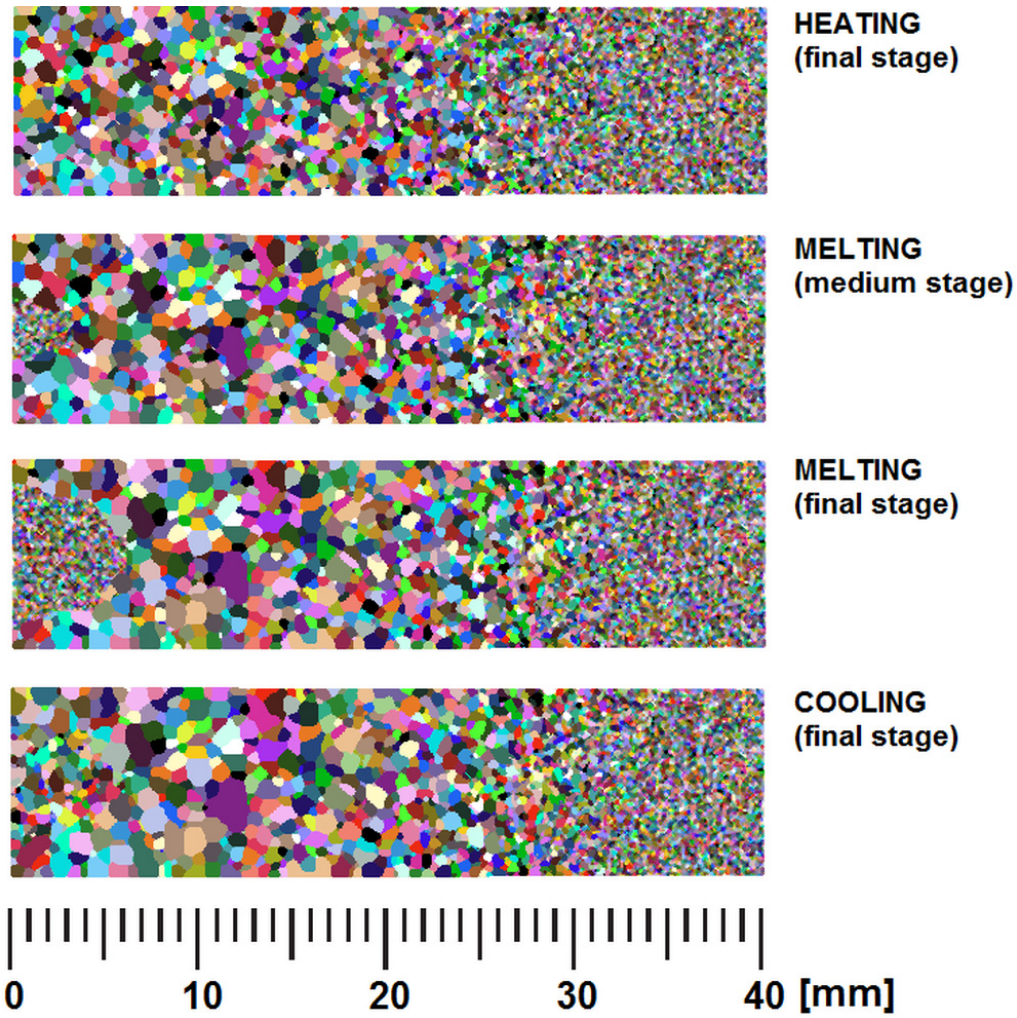

Fig. 17. Virtual macrostructure of the sample in the longitudinal section in the sample axis for the selected four process stages (*third degree* boundary mobility function)

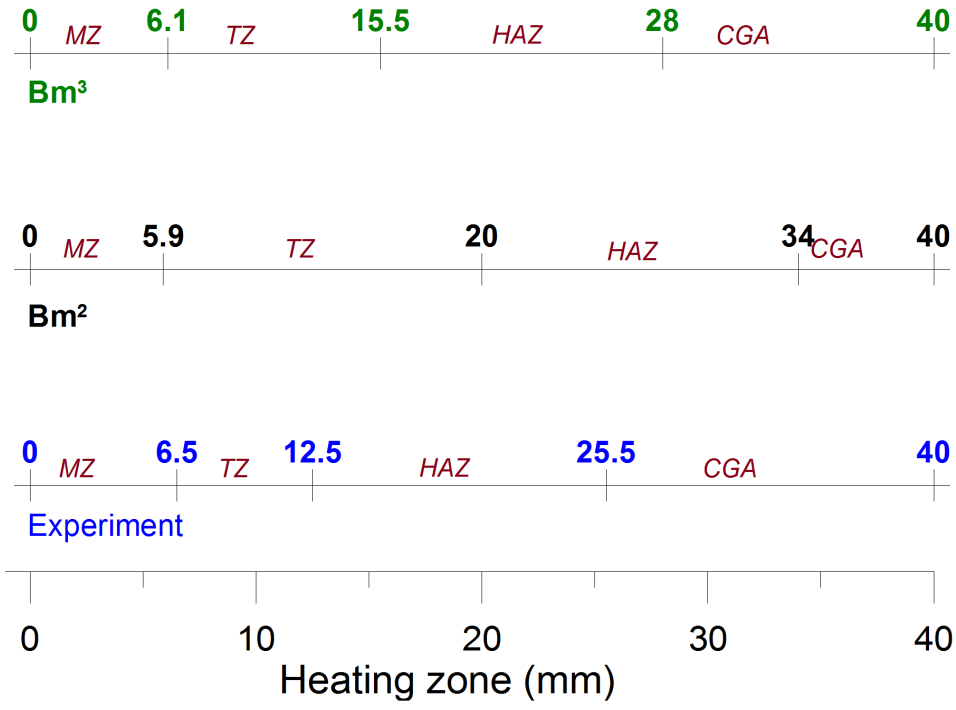

Fig. 18. Estimated ranges of zones with a diverse dynamics of grain growth obtained by experiment and numerical computing

5. Conclusion

The paper presents main assumptions of a multi-scale model dedicated to simulations of resistance heating combined with the potential melting and controlled cooling of steel samples. The developed solution combines the advantages of the finite element method for predicting temperature fields within the sample volume and the Monte Carlo methods for estimating zones with diversified dynamics of grain growth. The two models were coupled by the interpolation of node temperatures of the finite element mesh (the macro model) onto the Monte Carlo cells (micro model). At the present stage of the model development, feedback from the micro to the macro model has not been executed. The presented results of numerical simulations feature good compliance with experiments as regards predicting temperature fields. Coupling the macro model with the Monte Carlo micro model allowed also the range of occurrence of zones with a diverse dynamics of grain growth within the sample volume to be correctly estimated. Here, the proper selection of the scaling function degree has had a significant impact on the achieved result. It was selected experimentally by comparing macrostructures obtained by experiment and the numerical simulation. Very long computing times, reaching up to a dozen or so weeks if the whole sample is considered the solution domain are a negative feature of the developed solution. The numerical computing was performed using a workstation equipped with a processor Intel Core i7 Extreme CPU, 24 GB RAM and three cards NVIDIA GeFore GTX 760. At present the adaptation of the grain growth micro-model onto the computing platform using NVidia Graphical Processor Units (GPU) is in progress. The use of GPU will allow the computing times to be effectively shortened from over ten weeks to a few days.

Acknowledgment

1. The research work has been supported by the Polish National Science Centre, Decision number: DEC-2011/03/D/ST8/04041

2. Development of methods for increasing computational efficiency of micro model supported by AGH grant no. 11.11.110.593

REFERENCES

[1] M. Hojny, Modeling steel deformation in the semi-solid state: Advanced Structured Materials, Springer, Switzerland (2018).

[2] L. Zhang, H. Shen, Y. Rong, Mat. Sc. and Eng. **466** (1-2), 71-78 (2007).

[3] A. Kalaki, M. Ketabchi, J. of Mat. Eng. and Tech. **1** (3), 41-45 (2013).

[4] T. Haga, S. Suzuki, J. Mat. Proc. Tech. **143-144** (1), 895-900 (2003).

[5] T. Haga, K. Tkahashi, M. Ikawa, J. Mat. Proc. Tech. **153-154** (2), 42-47 (2004).

[6] S.B. Hassas-Irani, A. Zarei-Hanzaki, B. Bazaz, A.Roostaei, Materials and Design **46**, 579-587 (2013).

[7] Chenyang Zhang, Shengdun Zhao, Guanhai Yan, Yongfei Wang, Journal of Engineering Manufacture **232** (3), 487-498 (2018).

[8] J. Wang et al., Solid State Phenomena **256**, 31-38 (2016).

[9] C.H. Shashikanth, M.J. Davidson, Materials at High Temperatures **32** (6), 541-550(2015).

[10] Katti Bharath, Asit Kumar Khanra, M. J. Davidson, Advances in Materials and Metallurgy, 101-114 (2019).

[11] C. H. Shashikanth, M. J. Davidson, Materials at High Temperatures **31** (3), 274-281 (2014).

[12] J.C. Álvarez Hostos et al., International Journal of Plasticity **103**, 119-142 (2018).

[13] R. Kopp, J. Choi, D. Neudenberger, J. Mat. Proc. Tech. **135**, 317-323 (2003).

[14] M. Modigell, L. Pape, M. Hufschmidt, Steel Research Int. **75**, 506-512 (2004).

[15] M. Hufschmidt, M. Modigell, J. Petera, Steel Research Int. **75**, 513-518 (2004).

[16] Y.L. Jing, S. Sumio, Y. Jun, J. Mat. Proc. Tech. **161**, 396-406 (2005).

[17] S. D. Jin, O.K. Hwan, Acta Materialia **50**, 2259-2268 (2002).

[18] P. Bereczki et al., Materials Performance and Characterization, ASTM, USA (2015).

[19] N. Szczygioł, Sol. of Mat. and Al. **30**, 221-232(1997).

[20] R.W. Lewis, P.M. Roberts, App. Sc. Res. **44**, 61-92(1987).

[21] Ł. Madej, Development of the modelling strategy for the strain localization simulation based on the digital material representation, AGH, Cracow (2010).